Dynamic Control of Chiral Space in a Catalytic Asymmetric Reaction Using a Molecular Motor

Jiaobing Wang, *et al.*

Science **331**, 1429 (2011);
DOI: 10.1126/science.1199844

propulsion, as a boiler feedwater deoxygenating agent, and in the manufacture of foamed plastics, pharmaceuticals, and biodegradable pesticides and herbicides (*38*). However, with worldwide production capacity estimated to be ~200,000 metric tons/year in 2007, the limited production volume and limited applications make current pricing less relevant. Hydrazine production colocated with recycle plants would reduce the transportation and storage costs and reduce the cost of hydrazine further, although a more efficient method for hydrazine synthesis would be of greater benefit.

The overall reaction cycle, including the production of hydrazine, is summarized in Fig. 3. In this scheme, the N_2 released from the N_2H_4 can be rehydrogenated to NH_3 and subsequently converted to N_2H_4. Although synthetic procedures such as the Olin-Raschig process produce hydrazine in high yields and great efficiency, we can begin to look to the future and think about a new route to hydrazine production. In conjunction with an AB-regeneration plant, in situ N_2H_4 production from NH_3 does not require high conversion rates to produce a N_2H_4/NH_3 feed for AB regeneration. In this scheme, the only material consumed is hydrogen, the production of which is widely recognized as the second major technical challenge for the hydrogen economy.

References and Notes

1. F. H. Stephens, V. Pons, R. Tom Baker, *Dalton Trans.* **2007** (no. 25), 2613 (2007).
2. S. Orimo, Y. Nakamori, J. R. Eliseo, A. Züttel, C. M. Jensen, *Chem. Rev.* **107**, 4111 (2007).
3. L. Wang, R. T. Yang, *Energy Environ. Sci.* **1**, 268 (2008).
4. M. E. Bluhm, M. G. Bradley, R. Butterick III, U. Kusari, L. G. Sneddon, *J. Am. Chem. Soc.* **128**, 7748 (2006).
5. M. C. Denney, V. Pons, T. J. Hebden, D. M. Heinekey, K. I. Goldberg, *J. Am. Chem. Soc.* **128**, 12048 (2006).
6. R. J. Keaton, J. M. Blacquiere, R. T. Baker, *J. Am. Chem. Soc.* **129**, 1844 (2007).
7. F. H. Stephens, R. T. Baker, M. H. Matus, D. J. Grant, D. A. Dixon, *Angew. Chem. Int. Ed.* **46**, 746 (2007).
8. V. Pons *et al.*, *Chem. Commun. (Camb.)* **2008** (no. 48), 6597 (2008).
9. L. G. Sneddon, "Amineborane Hydrogen Storage," Department of Energy Hydrogen Program Review, 2006 (www.hydrogen.energy.gov/pdfs/review06/st_3_sneddon.pdf).
10. L. G. Sneddon, "Amineborane-Based Chemical Hydrogen Storage," Department of Energy Hydrogen Program Review, 2007 (www.hydrogen.energy.gov/pdfs/review07/st_27_sneddon.pdf).
11. S. Hausdorf, F. Baitalow, G. Wolf, F. O. R. L. Mertens, *Int. J. Hydrogen Energy* **33**, 608 (2008).
12. P. V. Ramachandran, P. D. Gagare, *Inorg. Chem.* **46**, 7810 (2007).
13. B. L. Davis *et al.*, *Angew. Chem.* **48**, 6812 (2009).
14. N. C. Smythe, J. C. Gordon, *Eur. J. Inorg. Chem.* **2010** (no. 4), 509 (2010).
15. C. W. Hamilton, R. T. Baker, A. Staubitz, I. Manners, *Chem. Soc. Rev.* **38**, 279 (2009).
16. G. Alcaraz, S. Sabo-Etienne, *Angew. Chem. Int. Ed.* **49**, 7170 (2010).
17. C. A. Jaska, K. Temple, A. J. Lough, I. Manners, *Chem. Commun. (Camb.)* (11), 962 (2001).
18. C. A. Jaska, K. Temple, A. J. Lough, I. Manners, *J. Am. Chem. Soc.* **125**, 9424 (2003).
19. A. Staubitz *et al.*, *J. Am. Chem. Soc.* **132**, 13332 (2010).
20. P. J. Fazen *et al.*, *Chem. Mater.* **7**, 1942 (1995).
21. P. J. Fazen, J. S. Beck, A. T. Lynch, E. E. Remsen, L. G. Sneddon, *Chem. Mater.* **2**, 96 (1990).
22. M. H. Matus, K. D. Anderson, D. M. Camaioni, S. T. Autrey, D. A. Dixon, *J. Phys. Chem. A* **111**, 4411 (2007).
23. C. R. Miranda, G. Ceder, *J. Chem. Phys.* **126**, 184703/1-11 (2007).
24. J. Baumann, thesis, *Physikalisch-chemische Untersuchungen zur Wasserstoffabgabe von BNH-Verbindungen*, 2003, Technische Universität Bergakademie, Freiberg, Germany.
25. G. Wolf, "Hydrogen storage with novel Nanomaterials," in *361. W. E.-Heraeus-Seminar on Hydrogen Storage with Novel Nanomaterials*, 23 to 27 October 2005, Bad Honnef, Germany (www.h-workshop.uni-konstanz.de/pdf/Wolf_Gert.pdf).
26. A. D. Sutton *et al.*, *Chem. Commun. (Camb.)* **46**, 148 (2010).
27. A. K. Burrell, "Chemical Hydrogen Storage R&D at Los Alamos National Laboratory," DOE Hydrogen Program Review, 2009 (www.hydrogen.energy.gov/pdfs/review09/st_17_burrell.pdf).
28. Materials and methods are available as supporting material on *Science* Online.
29. J. Goubeau, E. Ricker, *Z. Anorg. Allg. Chem.* **310**, 123 (1961).
30. T. Hügle, M. F. Kühnel, D. Lentz, *J. Am. Chem. Soc.* **131**, 7444 (2009).
31. J. Tomasi, B. Mennucci, R. Cammi, *Chem. Rev.* **105**, 2999 (2005).
32. A. Klamt, G. Schüürmann, *J. Chem. Soc., Perkin Trans. 2* 799 (1993).
33. M. J. Frisch *et al.*, *Gaussian 03*, Revision C. 02 (Gaussian, Inc., Wallingford, CT, 2004).
34. E. J. Baerends *et al.*, ADF2008.01, SCM, Amsterdam, 2008.
35. G. te Velde *et al.*, *J. Comput. Chem.* **22**, 931 (2001).
36. F. Baitalow, J. Baumann, G. Wolf, K. Jaenicke-Rößler, G. Leitner, *Thermochim. Acta* **391**, 159 (2002).
37. A. G. Baboul, L. A. Curtiss, P. C. Redfern, K. J. Raghavachari, *J. Chem. Phys.* **110**, 7650 (1999).
38. E. W. Schmidt, *Hydrazine and its Derivatives: Preparation, Properties, Applications* (Wiley-Interscience, New York, ed. 2, 2001).

39. This work was funded by the U.S. Department of Energy, Office of Energy Efficiency and Renewable Energy. The authors and Los Alamos National Laboratory have filed a patent on the methods presented herein. We thank L. Sneddon for invaluable discussions.

Supporting Online Material

www.sciencemag.org/cgi/content/full/331/6023/1426/DC1
Materials and Methods
Figs. S1 to S5
Tables S1 to S4
References

13 October 2010; accepted 31 January 2011
10.1126/science.1199003

Dynamic Control of Chiral Space in a Catalytic Asymmetric Reaction Using a Molecular Motor

Jiaobing Wang and Ben L. Feringa*

Enzymes and synthetic chiral catalysts have found widespread application to produce single enantiomers, but in situ switching of the chiral preference of a catalytic system is very difficult to achieve. Here, we report on a light-driven molecular motor with integrated catalytic functions in which the stepwise change in configuration during a 360° unidirectional rotary cycle governs the catalyst performance both with respect to activity and absolute stereocontrol in an asymmetric transformation. During one full rotary cycle, catalysts are formed that provide either racemic (*R*,*S*) or preferentially the *R* or the *S* enantiomer of the chiral product of a conjugate addition reaction. This catalytic system demonstrates how different molecular tasks can be performed in a sequential manner, with the sequence controlled by the directionality of a rotary cycle.

The ease with which nature controls the chirality of the product of an enzymatic reaction has spurred and inspired the development of synthetic compounds that enantioselectively catalyze a myriad of asymmetric transformations (*1*, *2*). The precise spatial arrangement of amino acid and cofactor subunits in a highly dynamic setting is the key to enantioselectivity achieved by enzymes, yet the chirality of the active site environment is set by the inherent chirality of the constituent amino acid building blocks. As a result, it is very challenging to switch an enzyme's selectivity from favoring a product of one chiral sense to favoring its enantiomer, although genetic engineering and directed evolution approaches can be brought to bear in certain cases (*3*). By contrast, the comparative structural simplicity of synthetic asymmetric catalysts often allows facile preparation of both catalyst enantiomers, thereby enabling preparation of each product enantiomer individually (*4*). In addition, strategies that allow for the formation of either product enantiomer from a single enantiomer of a catalyst have also been developed, for example, by changing the reaction conditions, including solvent or temperature, or by the addition of different Lewis acids (*5*, *6*). But can we go further; can we modulate

Centre for Systems Chemistry, Stratingh Institute for Chemistry and Zernike Institute for Advanced Materials, University of Groningen, Nijenborgh 4, 9747 AG, Groningen, Netherlands.

*To whom correspondence should be addressed. E-mail: b.l.feringa@rug.nl

the chiral sense of the space in which a catalyzed reaction takes place in a dynamic and responsive manner using an external stimulus?

Here, we show that an external signal, that is, light, can be used to control the chiral space in which a catalytic reaction takes place. In our design, a single enantiomer of a molecular catalytic system can be triggered in situ to produce a racemate, one enantiomer, or the other enantiomer of a chiral product on demand.

We demonstrate the basic principle of such a chiral catalytic system by exploiting the unique dynamic stereochemical features of unidirectional rotary molecular motors (*7*–*9*). During the individual steps of a rotary cycle of a light-driven molecular motor, the stereochemistry changes several times. This variability provides a scenario for the design of a motor with integrated catalytic functions in which the stereocontrol during the catalytic event can be alternated by light in a sequential manner. The individual chiral stages during the unidirectional rotary cycle dictate the ability of the catalyst to induce a preferred handedness in the product formed during an asymmetric transformation.

The design principle, in which motor and catalytic functions are integrated, is shown in Fig. 1 (top). A light-driven molecular motor is functionalized at the rotor and stator segments with moieties A and B, respectively, which can cooperate to form a bifunctional organocatalyst (*10*, *11*) when in proximity to each other. The helicity of the motor unit, which dictates the overall chirality of the system, changes during the 360° rotary cycle. Simultaneously, the precise positioning of the two catalytic moieties A and B in space, both with respect to distance and helical organization, is governed by rotor and stator orientation at each stage of the rotary cycle. A and B can be remote (stage I), in close proximity with *M* helicity (stage II), or in close proximity with *P* helicity (stage III). As a consequence, the cooperative effect of A and B and the preferred chiral sense induced in a transformation catalyzed by the system is modulated by the rotary cycle.

In contrast to other light-gated systems (*12*), this adaptive chiral catalyst allows for exquisite control over both catalytic activity and stereoselectivity in a concerted and fully reversible manner.

The structure of the molecular motor–based catalyst is shown in Fig. 1 (bottom). The molecule is a single enantiomer in which *R* denotes the absolute configuration at the methyl-substituted indanyl centers, *P* the helicity of the indane pair, and trans the orientation of the two pendant functional groups (A and B in Fig. 1) about the central olefin. The design features a chiral overcrowded alkene that can perform a unidirectional four-stage rotation cycle fueled by light irradiation (*7*, *13*, *14*). The catalytic moieties are modeled after recently developed organocatalysts (*15*–*17*) and are connected to the motor via para-phenyl spacers at the stator and rotor units of the motor. They comprise a DMAP (dimethylaminopyridine) Brønsted base (A) and a thiourea hydrogen-bonding donor group (B) to ensure cooperative action in organocatalytic Michael additions (*16*, *17*). However, before addressing the issue of control of catalytic function, the proper operation of the unidirectional rotary motor has to be established.

The syntheses of (*2R*,*2′R*)-(*P*,*P*)-*trans*-**1** and its enantiomer (*2S*,*2′S*)-(*M*,*M*)-*trans*-**1** are detailed in figs. S1 to S6 and notes S1 to S3. Unless indicated otherwise, the (*2R*,*2′R*)-(*P*,*P*) enantiomer was used to obtain the results that follow. Unidirectional clockwise rotation of the rotor with respect to the stator in motor **1** was confirmed by a combination of ultraviolet-visible (UV-vis), circular dichroism (CD), and proton nuclear magnetic resonance (^{1}H-NMR) spectroscopy and chiral high-performance liquid chromatography (HPLC). Upon exposure of enantiomerically pure (*P*,*P*)-*trans*-**1**, dissolved in tetrahydrofuran (THF), to UV irradiation (λ^{irr} = 312 nm) at 20°C, the intensity of the absorption band at 300 nm decreases in concert with the emergence of a red-shifted absorption at 360 nm (Fig. 2A). The spectral change was assigned to a (*P*,*P*)-*trans*-**1** → (*M*,*M*)-*cis*-**1** interconversion (Fig. 2J) (Φ^{iso} = 0.37) with a photostationary state comprising >99% of (*M*,*M*)-*cis*-**1**. The formation of (*M*,*M*)-*cis*-**1** was also evident from chiral HPLC (see fig. S7) and ^{1}H-NMR analysis (Fig. 2I) and the observed CD spectral changes (Fig. 2E) typically associated with the *P*,*P* to *M*,*M* helix inversion (*7*). When the solution of (*M*,*M*)-*cis*-**1** was subsequently heated at 70°C for 40 min, a thermal isomerization step (standard Gibbs energy of activation $\Delta^{\ddagger}G°$ = 104.1 kJ/mol; for the kinetic data and analysis, see fig. S8) resulted in the formation of (*P*,*P*)-*cis*-**1** (Fig. 2J), as indicated by the decrease in absorption at 360 nm (Fig. 2B). The concomitant helix inversion of the cis isomer of **1** from *M*,*M* to *P*,*P* is supported by ^{1}H-NMR (Fig. 2I), chiral HPLC (see fig. S7), and CD (Fig. 2F) measurements. Quantitative analysis of these data revealed that 76% of (*P*,*P*)-*cis*-**1** was obtained after this isomerization step. Two subsequent photochemical and thermal isomerization steps, 3 and 4 (Fig. 2J), of (*P*,*P*)-*cis*-**1** resulted in the formation of the original (*P*,*P*)-*trans*-**1** isomer, completing the four-stage cycle. In this final sequence, the photochemical (*P*,*P*)-*cis*-**1** to (*M*,*M*)-*trans*-**1** isomerization (λ^{irr} = 312 nm, –60°C, Φ^{iso} = 0.18, 81%) provides a highly unstable isomer that undergoes rapid (–10°C, 100%) unidirectional thermal isomerization to the initial (*P*,*P*)-*trans*-**1** isomer. Again the structural changes and helix inversions during these isomerization processes could be followed by UV-vis (Fig. 2, C and D) and CD (Fig. 2, G and H) spectroscopy and chiral HPLC (see fig. S7), confirming that the initial (*P*,*P*)-*trans*-**1** isomer was formed after the complete cycle.

The UV-vis spectral changes during these isomerizations show distinct isosbestic points (332 nm, step 1; 329 nm, step 2; 318 nm, step 3; 326 nm, step 4), indicating selective unimolecular processes. Each photoisomerization is accompanied by a red-shifted absorption consistent with the formation of a high-energy isomer due to enhanced strain in the helical structure. The subsequent energetically downhill thermal isomerization steps result in a more relaxed structure and govern the unidirectional nature of the entire rotary cycle.

Having established the four-step unidirectional rotary cycle of **1**, we investigated its performance as a chiral organocatalyst, using the enantioselective Michael addition of 2-methoxy thiophenol **2** to cyclohexenone **3** as a model reaction (Fig. 3A) (*17*). Product formation was monitored by ^{1}H-NMR in CD_2Cl_2 at –15°C with a catalyst loading as low as 0.3 mole percent (mol %) (see note S4). The enantiomeric ratio (e.r.) and absolute configuration of product **4** were determined by chiral HPLC (see Fig. 3, C to E). When the (*P*,*P*)-*trans*-**1** isomer

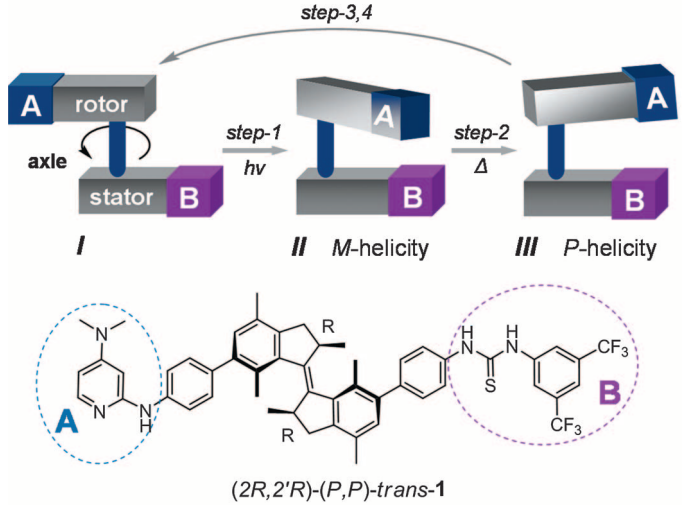

Fig. 1. Schematic illustration of an integrated unidirectional light-driven molecular motor and bifunctional organocatalyst (top) and the molecular structure of (*2R*,*2′R*)-(*P*,*P*)-*trans*-**1** (bottom). The motor comprises a rotor and stator connected by an alkene moiety that functions as the axle. A and B are DMAP and thiourea catalytic groups, respectively, that can cooperate as Brønsted base and hydrogen bond donor in an organocatalytic conjugate addition. Clockwise rotation (seen from the stator side) of the rotor around the axle, by photochemically and thermally induced steps, controls the position and helical orientation of the catalytic groups A and B, providing sequentially catalysts I, II, and III with different activities and stereoselectivities. The last two isomerization steps [steps 3 and 4 of the 360°C rotary cycle (see Fig. 2)] reset the catalyst to its initial stage I.

(Fig. 2J) was used as a catalyst, racemic (*R*,*S*)-thiol adduct **4** (Fig. 3C) was obtained in a slow reaction (7% yield after 15 hours). The low activity of the trans isomer of motor **1** is attributed to the unfavorable orientation of the DMAP and thiourea moieties on the motor scaffold, which precludes the operation of cooperative bifunctional catalysis. In sharp contrast, after photoisomerization, the Michael addition proceeds significantly faster as the (*M*,*M*)-*cis*-**1** isomer [stable under the reaction conditions without noticeable isomerization; half-time ($t^{1/2}$) = 120 days at 0°C] provides adduct **4** in 50% yield under the same conditions. More remarkable is the selective formation of the (*S*) enantiomer of adduct **4** with an e.r. of 75/25 (*S*/*R*) (Fig. 3D). The next isomer (*P*,*P*)-*cis*-**1** accelerates the addition reaction even more (83% yield in 15 hours) and exhibits an inversion in enantioselectivity, providing the (*R*) enantiomer of **4** with an e.r. of 23/77 (*S*/*R*) (Fig. 3E). The relative rates of product formation for the three catalysts (*P*,*P*)-*trans*-**1**, (*M*,*M*)-*cis*-**1**, and (*P*,*P*)-*cis*-**1** are displayed in Fig. 3B (see also fig. S9). The asymmetric Michael addition can be switched on in situ by irradiating the catalyst (*P*,*P*)-*trans*-**1** at 312 nm [to form (*M*,*M*)-*cis*-**1**] in the presence of reactants **2** and **3**, and a significant rate enhancement (40% yield in 15 hours) and comparable stereocontrol (e.r., 74/26, *S*/*R*) are observed (see fig. S10).

From these data, it is evident that the cis isomers of motor **1** display a strongly enhanced catalytic activity compared with *trans*-**1**. Stereocontrol is not observed at all for the trans isomer of motor **1**, in contrast to the cis isomers. This molecular motor–based organocatalyst has the distinct property that photoisomerization can be used to modulate both catalytic activity and the enantioselectivity. Based on mechanistic studies

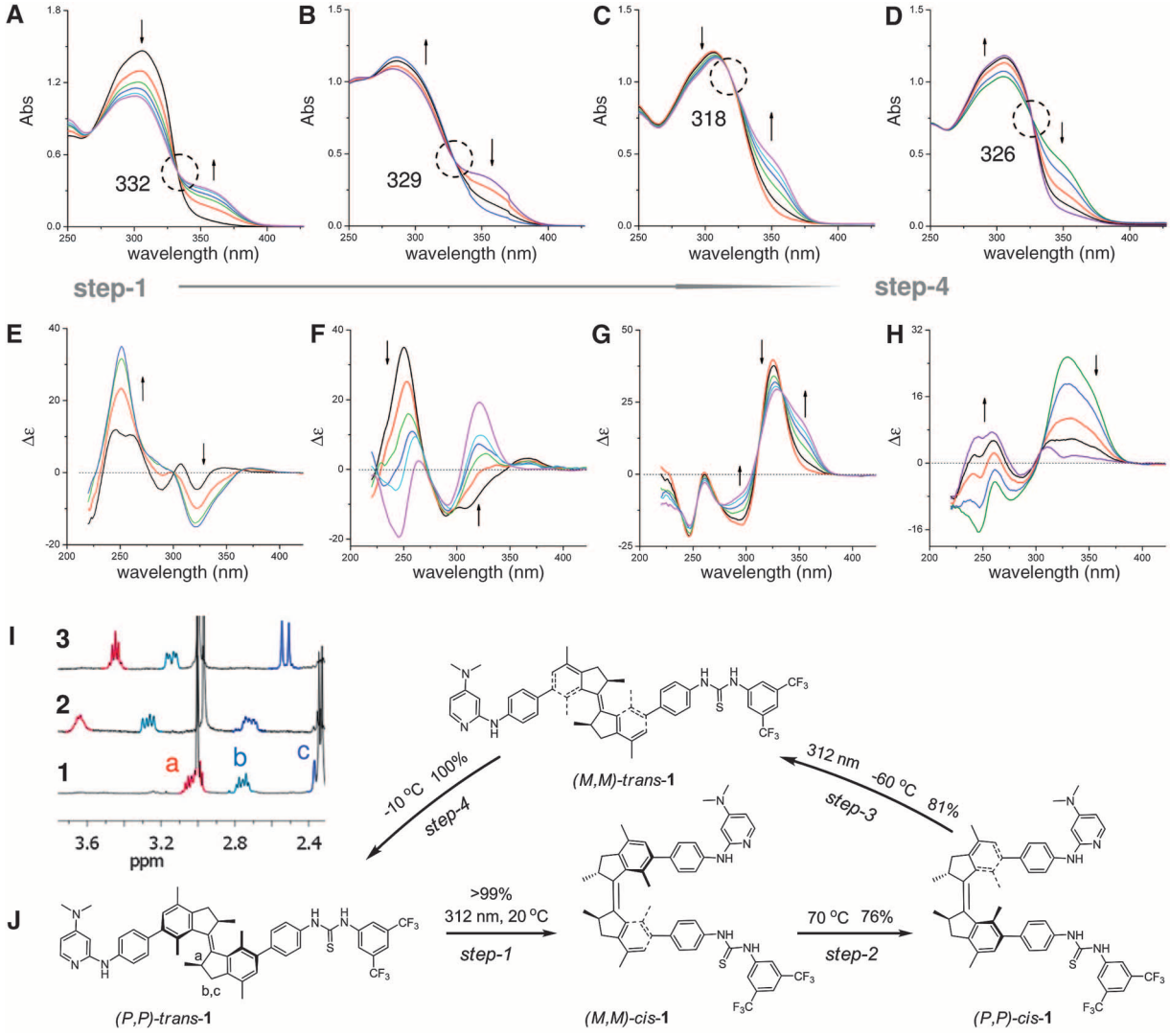

Fig. 2. UV-vis (A to D) and CD (E to H) spectral changes of compound **1** (2.0×10^{-5} M) in each isomerization process of the four-step unidirectional rotary cycle (J) fueled by UV irradiation and thermal energy. (**A**) UV-vis spectral changes during step 1 upon irradiation at 312 nm ($\Phi^{iso} = 0.37$) in THF at 20°C; isosbestic points are indicated with circles. (**B**) UV-vis spectral changes during step 2 on heating in THF/isopropanol at 70°C. (**C**) UV-vis spectral changes during step 3 on irradiation at 312 nm ($\Phi^{iso} = 0.18$) in THF at –60°C. (**D**) UV-vis spectral changes during step 4 ($t^{1/2} = 57$ min) in THF at –10°C. (**E** to **H**) The corresponding CD spectral changes during each of the four isomerization steps, respectively. Spatial orientation of the catalytic groups is controlled by the directional rotary motion of the molecular motor (**J**). Step 1: Starting from (*P*,*P*)-*trans*-**1**; a photoisomerization ($\lambda^{irr} = 312$ nm) provides (*M*,*M*)-*cis*-**1** in which helix inversion (from *P* to *M*) has occurred and the two catalytic groups are brought into close proximity. Step 2: A thermal helix inversion (70°C) provides (*P*,*P*)-*cis*-**1**, and the two catalytic units remain in close proximity while a helix inversion from *M* to *P* takes place. Steps 3 and 4: A photochemical step followed by thermal isomerization reset the original structure (*P*,*P*)-*trans*-**1** via the intermediacy of isomer (*M*,*M*)-*trans*-**1**, which was not studied as a catalyst due to low thermal stability. The partial ^{1}H-NMR (CD_2Cl_2) spectra of compounds (*P*,*P*)-*trans*-**1**, (*M*,*M*)-*cis*-**1**, and (*P*,*P*)-*cis*-**1** are shown in (**I**) 1 to 3, respectively [for the assignment of the protons, see (J), (*P*,*P*)-*trans*-**1**; singlet at 3.0 parts per million represents NMe_2 protons].

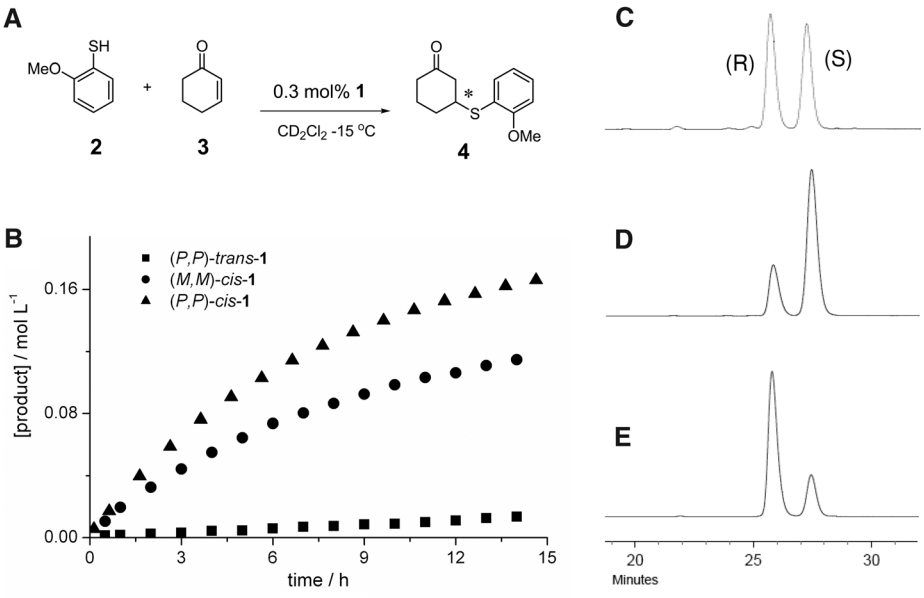

Fig. 3. Catalytic performance of compound **1** for the Michael addition of **2** (0.2 M) to **3** (0.2 M) to give chiral adduct **4**. (**A**) Reaction scheme and conditions. (**B**) Reaction kinetics followed by measuring product formation with in situ ^{1}H-NMR spectroscopy. (**C** to **E**) Chiral HPLC traces of the reaction product **4** using catalyst (*P*,*P*)-*trans*-**1** (e.r., *S*/*R*, 49/51), (*M*,*M*)-*cis*-**1** (e.r., *S*/*R*, 75/25), and (*P*,*P*)-*cis*-**1** (e.r., *S*/*R*, 23/77), respectively.

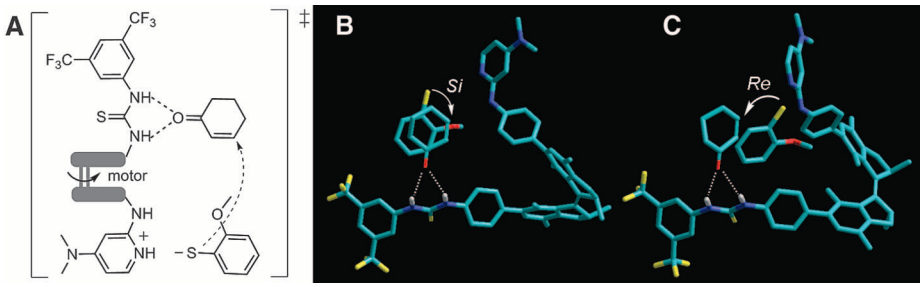

Fig. 4. Proposed ternary complex (**A**) involved in the mechanism of thiol addition to enone catalyzed by **1** and the energy-minimized structures for the asymmetric Michael addition (B and C) obtained using Hyperchem 8.0 (RM1). (**B**) Catalyst (*2R*,*2′R*)-(*M*,*M*)-*cis*-**1**; thiol addition to the Si face is favored (marked with arrow) to give the product (*S*)-**4**. (**C**) Catalyst (*2R*,*2′R*)-(*P*,*P*)-*cis*-**1**; thiol addition to the Re face is favored to give the product (*R*)-**4**. In the trans isomer (not shown), the catalytic units are pointed antiparallel to each other, precluding bifunctional activation (see fig. S11).

of bifunctional organocatalysts for thiol addition (*10*, *17*, *18*), it is proposed that this transformation (Fig. 4A) involves an activation of the enone through hydrogen bonding with the thiourea and deprotonation of the thiol nucleophile ($pK_a = 6.6$) by DMAP ($pK_a = 9.7$). The experimental observations suggest that the motor rotation not only controls the chirality of the entire system but also gears the catalytically active units to cooperate. In the trans isomer, due to the distant orientation of the thiourea and DMAP groups, no cooperative effect is possible, resulting in low catalytic activity. Basic molecular modeling studies were performed to rationalize the reversal in absolute stereochemistry of product **4** on shifting from catalyst (*M*,*M*)-*cis*-**1** to (*P*,*P*)-*cis*-**1** (Fig. 4, B and C).

The energy-minimized structure (see note S5) of the ternary complex comprising catalyst (*2R*,*2′R*)-(*M*,*M*)-*cis*-**1**, thiol **2**, and enone **3** (Fig. 4B) shows that thiol addition to the Si face of cyclohexenone is favored to give product **4** with the (*S*) configuration in accordance with experimental observation. Addition to the Re face is hampered by severe steric hindrance along the preferred Bürgi-Dunitz trajectory for conjugate addition (*19*). In contrast, when the (*2R*,*2′R*)-(*P*,*P*)-*cis*-**1** catalyst is employed (Fig. 4C), thiol addition to the Re face is more favorable, yielding product **4** with the (*R*)-absolute configuration.

It should be noted that the helicity (*P* or *M*) and directionality (clockwise or counterclockwise) of rotation of the molecular motor is governed by the chirality of the stereogenic centers (*R* or *S*) in the motor unit. The helicity (*P* or *M*) of the motor in turn dictates the spatial orientation of the catalytic groups and, as a consequence, the configuration (*R* or *S*) of the newly formed stereogenic center in the product **4** of the enantioselective catalytic event. This interdependence implies that on starting with (*2R*,*2′R*)-(*P*,*P*)-*trans*-**1** (Fig. 2), a clockwise rotary cycle provides sequentially racemic (*R*,*S*)-, (*S*)-, and (*R*)-product **4** (Fig. 3, C to E) before returning to produce racemic product after a full rotary cycle.

To further explore this delicate stereochemical interplay, the enantiomer of molecular motor **1**, with the (*2S*,*2′S*) configuration at the stereogenic centers, was examined. Because the (*2S*,*2′S*)-(*M*,*M*)-*trans*-**1** motor is now the starting point, a counterclockwise rotary cycle is induced upon photochemical and thermal isomerization, providing sequentially racemic (*R*,*S*)-, (*R*)-, and (*S*)-product **4** before returning to produce racemic product after a full rotary cycle (see fig. S12).

Coupling of unidirectional switching to catalytic function, as demonstrated here, may prove to be a key design tool in the construction of future catalysts that can perform multiple tasks in a sequential manner.

References and Notes

1. V. Gotor, I. Alfonso, E. García-Urdiales, Eds., *Asymmetric Organic Synthesis with Enzymes* (Wiley-VCH, Weinheim, Germany, 2008).
2. E. N. Jacobsen, A. Pfaltz, H. Yamamoto, Eds., *Comprehensive Asymmetric Catalysis I-III* (Springer, Berlin, 1999).
3. T. M. Penning, J. M. Jez, *Chem. Rev.* **101**, 3027 (2001).
4. H. U. Blaser, E. Schmidt, Eds., *Asymmetric Catalysis on Industrial Scale* (Wiley-VCH, Weinheim, Germany, 2004).
5. M. Sibi, M. Liu, *Curr. Org. Chem.* **5**, 719 (2001).
6. Y. Sohtome, S. Tanaka, K. Takada, T. Yamaguchi, K. Nagasawa, *Angew. Chem. Int. Ed.* **49**, 9254 (2010).
7. N. Koumura, R. W. J. Zijlstra, R. A. van Delden, N. Harada, B. L. Feringa, *Nature* **401**, 152 (1999).
8. R. Eelkema *et al.*, *Nature* **440**, 163 (2006).
9. M. Schliwa, Ed., *Molecular Motors* (Wiley-VCH, Weinheim, Germany, 2003).
10. A. G. Doyle, E. N. Jacobsen, *Chem. Rev.* **107**, 5713 (2007).
11. D. W. C. MacMillan, *Nature* **455**, 304 (2008).
12. R. S. Stoll, S. Hecht, *Angew. Chem. Int. Ed.* **49**, 5054 (2010).
13. M. M. Pollard, A. Meetsma, B. L. Feringa, *Org. Biomol. Chem.* **6**, 507 (2008).
14. J. Wang, A. Kulago, W. R. Browne, B. L. Feringa, *J. Am. Chem. Soc.* **132**, 4191 (2010).
15. T. Okino, Y. Hoashi, Y. Takemoto, *J. Am. Chem. Soc.* **125**, 12672 (2003).
16. C. Rabalakos, W. D. Wulff, *J. Am. Chem. Soc.* **130**, 13524 (2008).
17. N. K. Rana, S. Selvakumar, V. K. Singh, *J. Org. Chem.* **75**, 2089 (2010).
18. H. Hiemstra, H. Wynberg, *J. Am. Chem. Soc.* **103**, 417 (1981).
19. E. V. Anslyn, D. A. Dougherty, Eds., *Modern Physical Organic Chemistry* (University Science Books, Sausalito, CA, 2006).

20. We thank G. Caroli for assistance with the molecular modeling studies and W. R. Browne for discussion. This project was supported by the Netherlands Organization for Scientific Research (NWO-CW) and European Research Council (ERC grant 227897).

Supporting Online Material

www.sciencemag.org/cgi/content/full/science.1199844/DC1
SOM Text
Figs. S1 to S12
References

1 November 2010; accepted 18 January 2011
Published online 10 February 2011;
10.1126/science.1199844